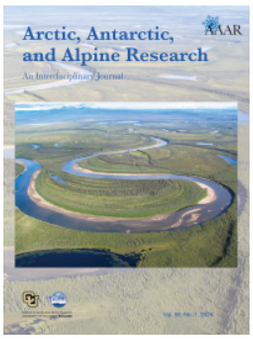

Taylor & Francis
Taylor & Francis Group

Arctic, Antarctic, and Alpine Research
An Interdisciplinary Journal

ISSN: (Print) (Online) Journal homepage: www.tandfonline.com/journals/uaar20

Ground-penetrating radar investigation of regolith thickness on a periglacial alpine summit flat, Uinta Mountains, Utah, USA

Jeffrey S. Munroe

To cite this article: Jeffrey S. Munroe (2024) Ground-penetrating radar investigation of regolith thickness on a periglacial alpine summit flat, Uinta Mountains, Utah, USA, Arctic, Antarctic, and Alpine Research, 56:1, 2322334, DOI: 10.1080/15230430.2024.2322334

To link to this article: https://doi.org/10.1080/15230430.2024.2322334

Published online: 14 Mar 2024.

ARCTIC, ANTARCTIC, AND ALPINE RESEARCH
2024, VOL. 56, NO. 1, 2322334
https://doi.org/10.1080/15230430.2024.2322334

Taylor & Francis
Taylor & Francis Group

Ground-penetrating radar investigation of regolith thickness on a periglacial alpine summit flat, Uinta Mountains, Utah, USA

Jeffrey S. Munroe

Department of Earth & Climate Sciences, Middlebury College, Middlebury, Vermont, USA

ABSTRACT

Summit flats are low-relief, gently sloping landforms common in periglacial mountain environments. Apart from at their edges where summit flats are truncated by glacial headwalls and at their crests where isolated tors are occasionally present, bedrock is typically mantled on a summit flat by a continuous layer of regolith. This study applied ground-penetrating radar (GPR) to survey the thickness of regolith on a summit flat in the Uinta Mountains (Utah, USA). More than 500 m of GPR data were collected along transects extending from the edge of the summit flat to the crest, as well as adjacent to a deep soil pit. Results indicate that the regolith thickness is quite variable, with a mean of 91 ± 38 cm when calculated with an appropriate radar velocity. Because the ground surface of the summit flat is notably smooth, the variability in thickness is a consequence of irregularities in the bedrock surface at depth, which is significantly rougher. Recognition that regolith thickness can vary considerably beneath an alpine summit flat has implications for soil formation, carbon storage, and the transmission and storage of shallow groundwater, as well as evolutionary models for periglacial mountain landscapes.

ARTICLE HISTORY
Received 5 December 2023
Revised 29 January 2024
Accepted 15 February 2024

KEYWORDS
Periglacial; summit flat; regolith; ground-penetrating radar; critical zone

Introduction

Many high-mountain environments feature periglacial landscapes that were above the limit of Pleistocene alpine glaciation. The dominant landform in these settings is often a low-relief, gently sloping, convex upland referred to as a "summit flat" (Small et al. 1997; R. S. Anderson 2002). The nearly flat appearance of these features presents a dramatic contrast with the precipitous slopes of the adjacent glacial valleys, rendering them conspicuous to any observer of mountain geomorphology. Early workers tended to consider summit flats as isolated remnants of formerly continuous, low-relief landscapes formed as pediments or peneplains (as reviewed in W. C. Bradley 1987). Other literature has explored the possibility that summit flats develop through expansion and coalescence of cryoplanation terraces (Nelson 1989; Czudek 1995). In this model, summit flats are time-transgressive landforms evolving in response to nivation (Thorn and Hall 2002; Nyland and Nelson 2020). Most recently, the development of techniques for the measurement of cosmogenic isotope abundances has allowed estimates of erosion rates on summit flats (Small et al. 1997; Small and Anderson 1998; Small, Anderson, and Hancock 1999), supporting numerical modeling efforts revealing that summit flats are predictable steady-state landforms produced under periglacial conditions (R. S. Anderson 2002; R. S. Anderson et al. 2006).

Descriptions of summit flats typically comment on the layer of regolith overlying the bedrock, where regolith refers to unconsolidated sediments that may or may not be organized into soil profiles. Statements such as "A regolith thickness of 1–2 m is common" (Small et al. 1997), "The regolith cover, where one can measure it, is on the order of 1 m thick and is quite uniform in thickness" (R. S. Anderson 2002, 38), or "... thin [roughly 1 m] but uniform" (R. S. Anderson et al. 2006, 400) are widespread. This regolith is likely a composite of material loosened from the underlying bedrock (Waroszewski et al. 2013), vestigial material from an older non-periglacial weathering regime (Mellor and Wilson 1989; Goodfellow 2012), and eolian additions of mineral dust (Litaor 1987; Muhs and Benedict 2006). Modeling efforts have proposed that the thickness of this regolith reflects a balance between rock breakdown and downslope transport through frost creep,

CONTACT Jeffrey S. Munroe jmunroe@middleury.edu Department of Earth & Climate Sciences, Middlebury College, Middlebury, VT 05753.

which ultimately delivers sediment to the edge of the summit flat, where it is lost into the glacial valley below by mass wasting (R. S. Anderson 2002). At larger spatial scales, therefore, the distribution of this regolith is in accordance with general diffusion models for soil formation and movement (Heimsath et al. 1999; Heimsath, Furbish, and Dietrich 2005).

Despite recognition that a layer of regolith is a universal characteristic of alpine summit flats, little is known about how the thickness of this material varies at smaller spatial scales. The frequent assertion that regolith on summit flats is uniform and ~1 m thick is actually based on a limited number of field observations (e.g., Small, Anderson, and Hancock 1999; Leopold et al. 2008). This is in contrast to non-alpine settings where a considerable literature exists on regolith and soil thickness (Heimsath et al. 1997; Phillips et al. 2005; Catani, Segoni, and Falorni 2010; Patton et al. 2018; Ferrell, Devine, and O'Geen 2023). Furthermore, the few studies that have specifically investigated regolith thickness in alpine settings have reported considerable inconsistency (Völkel, Leopold, and Roberts 2001; Leopold et al. 2008, 2013), emphasizing that the spatial variability of summit flat regolith thickness and its underlying controlling factors remain insufficiently studied.

This knowledge gap is significant because regolith plays important roles in the functioning of the "critical zone" (CZ), the thin skin of the Earth where geology, ecology, and hydrology intersect (Brantley, Goldhaber, and Ragnarsdottir 2007). For example, regolith is crucial for the storage and transmission of shallow groundwater (Holbrook et al. 2014; Sprenger et al. 2019) and can influence water chemistry (Checketts et al. 2020). Regolith forming at the interface between soil and bedrock serves as a source of plant-available nutrients (Brantley 2010) and a sink for elements sequestered by weathering (Chorover et al. 2007). Loose regolith is also the medium hosting most of the rhizosphere, upon which aboveground plants and the food webs they support are fundamentally reliant (Amundson et al. 2007). Periglacial soils and regolith, in particular, can be important reservoirs of carbon storage, aided by low mean annual temperatures that slow rates of decomposition and can facilitate the development of permafrost (Bockheim and Munroe 2014). All of these important functions are modulated to varying degrees by regolith thickness. Therefore, understanding of how the alpine CZ functions as a geoecological system would be improved by more detailed information about the spatial variability of regolith thickness derived from field studies.

In this study, I utilize ground-penetrating radar (GPR) to survey the thickness of regolith in an alpine summit flat locality that has been the focus of considerable previous research. GPR is a noninvasive geophysical technique effective for investigating depth to bedrock (Davis and Annan 1989; Doolittle et al. 2009) and is particularly appropriate for settings like the alpine CZ that are difficult to access and where techniques for direct observation such as trenching with heavy equipment would be too disruptive (Leopold et al. 2008). I use the results of the GPR surveys to quantify regolith thickness and address the assumption that thickness is uniform beneath the gently sloping summit flat surface.

Study area

Fieldwork for this project was conducted in the Uinta Mountains (Figure 1), a Laramide-age uplift of Precambrian metasedimentary rocks in northeastern Utah, USA (Sears, Graff, and Holden 1982; Hansen

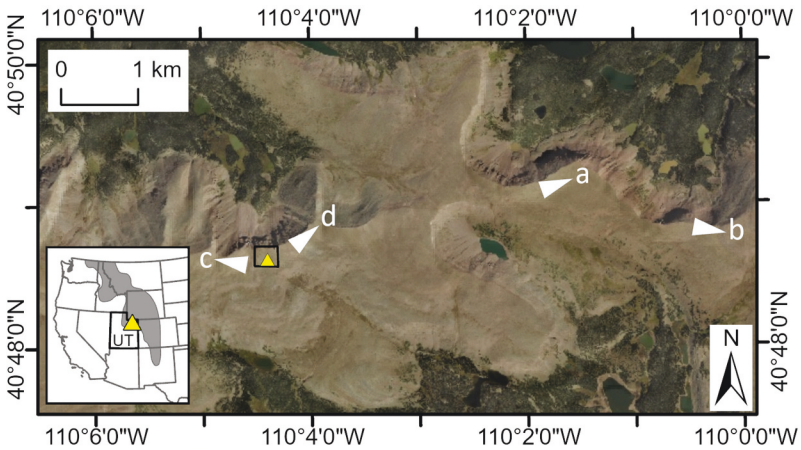

Figure 1. True color image of the Uinta Mountains from the NAIP program, 2014. The location of the Chepeta weather station is marked by a yellow triangle within the black box delineating the study area shown in Figure 3. Letters "a–d" refer to photographs in Figure 2; symbols display the approximate orientation of each of the images. Inset shows the position of the weather station (yellow triangle) within the Rocky Mountain system (dark gray) in western North America. The state of Utah (UT) is highlighted in black.

1986; Dehler et al. 2007). Maximum summit elevations in the Uinta Mountains (hereafter, the Uintas) are in excess of 4 km a.s.l., and the range was extensively glaciated during the Pleistocene (Munroe and Laabs 2009). On the basis of cosmogenic surface exposure dating and lacustrine sedimentary records, deglaciation of the Uintas was complete in the latest Pleistocene (Munroe and Laabs 2009); no alpine glaciers remain in these mountains today, although there are hundreds of active rock glaciers that likely contain perennial ice (Munroe 2018; Brencher, Handwerger, and Munroe 2021). Given lapse rates for mean annual temperature, permafrost is also likely present at the highest elevations in the Uintas (Obu et al. 2019).

Summit flats are well developed and extensive in the Uintas (Figures 1 and 2), as was noted by early researchers curious about the morphology and geologic history of these mountains (e.g., W. H. Bradley 1936). Previous work calculated that summit flats comprise 43 percent of the land area above 3,400 m and are more common toward the eastern end of the range where alpine glacial erosion was less severe (Munroe 2006). As is the case elsewhere in the Rocky Mountains (Small, Anderson, and Hancock 1999), there is no indication that summit flats in the Uintas were covered by erosive glacial ice; rocks and (rare) bedrock outcrops are not striated, and streamlined bedforms like roche moutonnées are absent. Although this is negative evidence and does not rule out the former presence of cold-based ice (e.g., Rea et al. 1996), it nonetheless strongly suggests that these uplands were not impacted by direct glacial erosion, likely because their windswept nature precluded snow accumulation.

The study area for this project is located in a broad saddle near the eastern end of the glaciated Uintas (Figures 1 and 2). The saddle has a crest elevation of ~3,695 m, which is >300 m above modern treeline, and slopes are generally <5°. The northern and southern limits of the summit flat are valleys enlarged by glaciers during the Pleistocene (Figure 1). Aside from the steep terrain at these boundaries, bedrock outcrops are absent on this summit flat. Instead, the surface is ornamented by well-developed and apparently fossil sorted stone polygons with diameters ~10 m (Munroe 2007). Toward the edges of the summit flat, polygons transition to stone stripes. Unvegetated and presumably active periglacial frost boils with diameters <1 m are also present. Otherwise, the ground surface is carpeted by low (<10 cm) *Acomastylis rossii* and other alpine plants.

This specific summit flat was selected for study because of the abundance of previous research conducted here. A passive dust sampler has been in operation at this site since 2011 (Munroe 2014), constraining rates of dust deposition (Munroe 2022). Soil profiles from this summit flat have been described and sampled, revealing the influence of long-term dust accumulation on pedogenesis (Munroe et al. 2015, 2020). Radiogenic isotope fingerprints ($^{87}Sr/^{86}Sr$ and ε_{Nd}) determined for modern dust and bedrock were used to estimate what fraction of the soil at this location was delivered by eolian processes (Munroe et al. 2020). Furthermore,

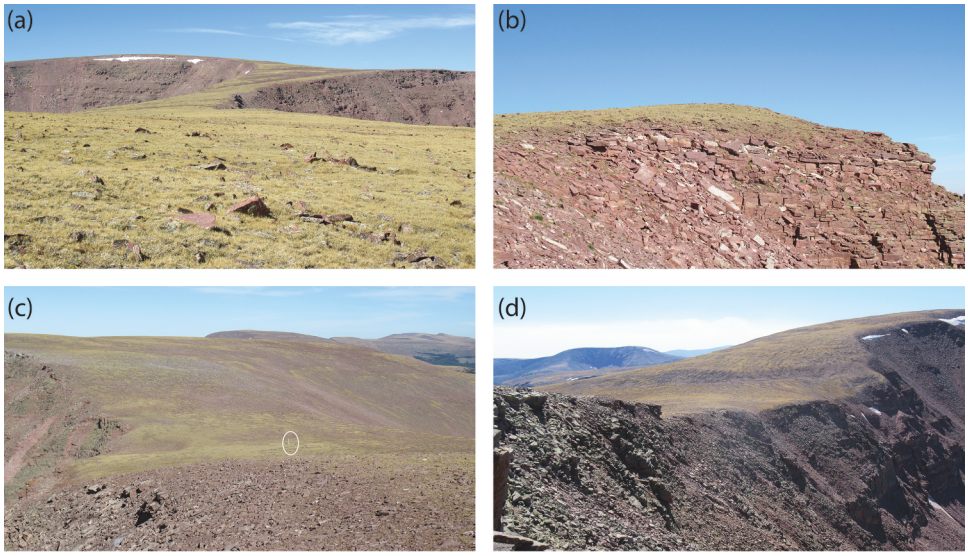

Figure 2. Photographs of summit flats in the Uinta Mountains. (a) Classic expression of periglacial summit flats truncated by alpine glacial erosion on both sides. (b) Exposed bedrock at the top of a glacial headwall capped by regolith at the edge of a summit flat. (c) The flat-floored saddle hosting the Chepeta site viewed from the west. The white oval highlights the Chepeta weather station. (d) The Chepeta site viewed from the northeast. Photopoint locations and orientation of each image are shown in Figure 1.

deeper regolith exposed at the top of the glacial headwall along the northern boundary of the summit flat is unexpectedly enriched in clay minerals, which have been studied to illuminate the role of allochthonous materials in soil formation (Munroe, Ryan, and Proctor 2021). Finally, a remote automated weather station (RAWS) has been in operation at this location since 1998 (Figure 1). Although there are gaps in the record due to occasional instrument malfunctions, the meteorological time series confirms the periglacial climate of this site, with a mean annual temperature of −2°C (Munroe 2006). The RAWS has the official designation CHPU1 (40.81110° N, 110.07470° W, 3,680 m) and the name "Chepeta"; thus, the location of this project is referred to as the Chepeta site.

Methods

Ground-penetrating radar surveys at the Chepeta site were conducted on 9 September 2021 with an SIR-4000 controller driving a 350HS antenna. Only 30 mm of precipitation was recorded in the three weeks prior to the fieldwork (0 mm in previous five days), and soil moisture conditions were dry. With the goal of investigating regolith expected to be on the order of a few meters thick, the 350 MHz system offered an acceptable compromise between resolution and depth of penetration, while also being portable enough to be backpacked to the study site. GPR data were collected by pulling the antenna across the ground surface at a walking pace along two 237-m-long transects marked at 18-m intervals. One transect (West) passed to the west of the Chepeta RAWS and the other to the east (East). The transects were not positioned directly along the fall line; rather, each started at the northern lip of the summit flat near where bedrock is exposed and continued to the southeast, up and over the broad crest before curving together to end at a common point (Figure 3). Each transect was surveyed twice to check for consistency. In addition, two perpendicular 10-m transects (Figure 3) were surveyed with their intersection point adjacent to a deep soil pit excavated in a previous study (Munroe et al. 2020). Data were also collected in stationary mode adjacent to this pit. For all transects, the GPR system collected 334 scans/second with 512 samples/scan. Spatial coordinates were automatically added to the datafile every 2 seconds from an Emlid Reach RS2 GPS receiver connected to the SIR-4000 (e.g., Doolittle et al. 2009), and reference marks were made in the record at each marked point along the transects.

Processing of the GPR data in RADAN v7.6 (2024) included aligning the first pulse of the radargram with the

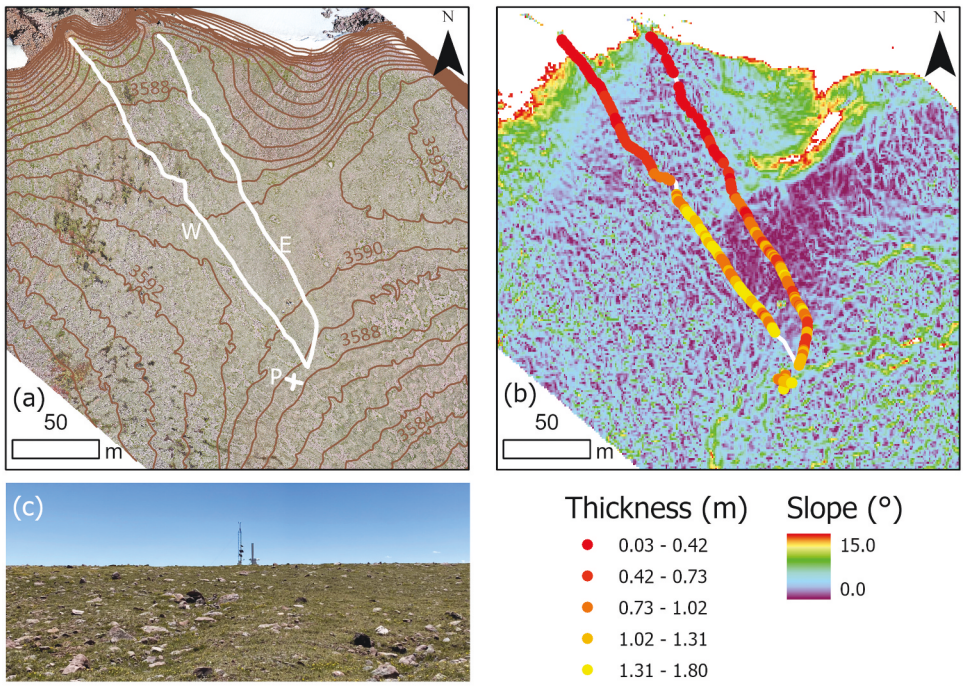

Figure 3. (a) Orthophoto mosaic of the Chepeta site derived from images collected by a UAV. Brown lines are 1 m contours. For clarity, contours are not shown on the steep headwall descending down into the cirque to the north. The GPR transects are shown as white lines: West (W), East (E), and the pair of crossing transects at the soil pit (P). (b) Slope map of the area shown in panel 'a'. Values clipped to ≤15° to highlight the summit flat surface. Inferred regolith thickness (in m) along the GPR transects is presented with overlapping colored dots. Regolith tends to be thicker under higher topography at the southern ends of the long transects where slopes are lower. (c) Photograph looking to the south toward the Chepeta weather station (on horizon) along the path of the East transect showing the typical surface of the summit flat in the study area.

ground surface; distance normalization to convert data to a constant horizontal scale using the 18-m reference points; background removal to eliminate linear, nonstratigraphic artifacts; high/low bandpass filtering to reduce noise; exponential range gain to accentuate deeper radar reflectors; topographic normalization based on the elevation component of the GPS data; and horizontal stacking to compress the long profiles for ease of viewing. To convert radar two-way travel times into depth, a relative dielectric permittivity value (ε_r) suitable for dry sandy soils (Martinez and Brynes 2001) that collapsed hyperbolic reflection from objects in the regolith (likely isolated boulders) was determined iteratively (Rønning 2023). This value was checked against the data for the crossing profiles collected near the soil pit (Figure 3) where bedrock was not encountered and subsequently used to migrate the radar data.

In both long transects, as well as the 10-m transects near the soil pit, a prominent continuous reflector was visible in the subsurface. This reflector represents an abrupt transition between materials with contrasting ε_r values. Points were manually digitized along this reflector at the position of the maximum positive amplitude. The depths of these points were then compared with the elevation of the overlying ground surface (from the GPS data) to compute the elevation of this reflector along the transects. Imprecision inherent in determining the vertical position of points along this reflector is estimated as ~20 cm, one-quarter of the radar wavelength at the antenna center frequency. Digitizing along the reflectors was repeated multiple times to determine that results were reproducible.

To produce a high-resolution base map and terrain model for the Chepeta site, the area was mapped with an uncrewed aerial vehicle (UAV, drone). The UAV flew at an altitude of 90 m above the ground surface, adjusted in real time with respect to a 30-m digital elevation model (DEM), collecting 258 images covering an area of 8.24 ha with 80 percent overlap. Images were processed to yield an orthophoto mosaic with a resolution of 2.2 cm per pixel (Figure 3). Structure from motion analysis was implemented to generate a DEM with an average resolution of 10 cm. This DEM was used in a GIS to generate a hillshade and slope raster for the study area.

Results

The combination of GPR with integrated GPS receiver and UAV-based mapping successfully defined the morphology of the Chepeta site and revealed the dimensions of the regolith layer underlying the ground surface. The GPR data reveal an array of reflectors within the shallow subsurface (Figures 4 and 5). Particularly notable in all transects is a reflector, laterally continuous at the scale of one to tens of meters, distinguished by locally high amplitude (e.g., Doolittle et al. 2009). This reflector is interpreted to be the bedrock/regolith interface for several reasons. First, its continuity indicates that it is not a local feature within the regolith, such as a group of stones concentrated by cryoturbation. Second, the locally high amplitude of this reflector implies a strong ε_r contrast between two overlying materials, which is unlikely to be the case for a soil horizon or stratigraphic layering in the bedrock. Third, the reflector typically has a positive–negative–positive pattern, indicating a contrast between an overlying material with higher ε_r and a deeper material with lower ε_r, as would be the case in where soil and regolith with relatively higher clay content overlies sandstone bedrock. Finally, the depth of this reflector beneath the local ground surface varies in a wavy, erratic manner, which is not what would be expected for the water table (Doolittle et al. 2006).

Prominent hyperbolae visible in the GPR data, likely representing individual rocks dispersed within the finer regolith matrix, were iteratively determined to collapse at ε_r values between 6 and 8. Applying the higher end of this range to the radar data from near the soil pit (Figure 5), however, placed the apparent depth of the bedrock reflector shallower than the base of the pit (92 cm) where bedrock was not encountered (Munroe et al. 2020), suggesting that ε_r values greater than 6 might not be universally appropriate for the regolith at the Chepeta site. All radar profiles were therefore migrated with a ε_r of 6, corresponding to a radar velocity of 0.12 m/ns, typical for dry, sandy soils (Martinez and Brynes 2001).

To provide an uncertainty estimate for the regolith thickness, depths of the bedrock reflector (Figures 5 and 6) were calculated with ε_r values of 4, 6, and 8, all of which are reasonable for sandy materials with low water content (Martinez and Brynes 2001). In general, thickness is greater beneath the southern, higher part of the transects and thins to the north toward the edge of the summit flat (Figures 3–5). The area of greater thickness roughly corresponds with the part of the summit flat exhibiting gentler slopes (Figure 3). Overall average thickness is slightly greater along the West transect, with a mean 99 ± 44 cm with an ε_r of 6 (Figures 6 and 7). Along the East transect, the average is 76 ± 35 cm. Combining the data from both long transects and the crossing transects near the soil pit (Figure 3) yields a composite mean of 91 ± 38 cm. This average rises to 114 ± 49 cm at ε_r of 4 and falls to 80 ± 35 cm at ε_r of 8 (Figure 7). Uncertainty in the depth estimates arising from imprecision in digitizing points on the reflector is not explicitly considered because it is less

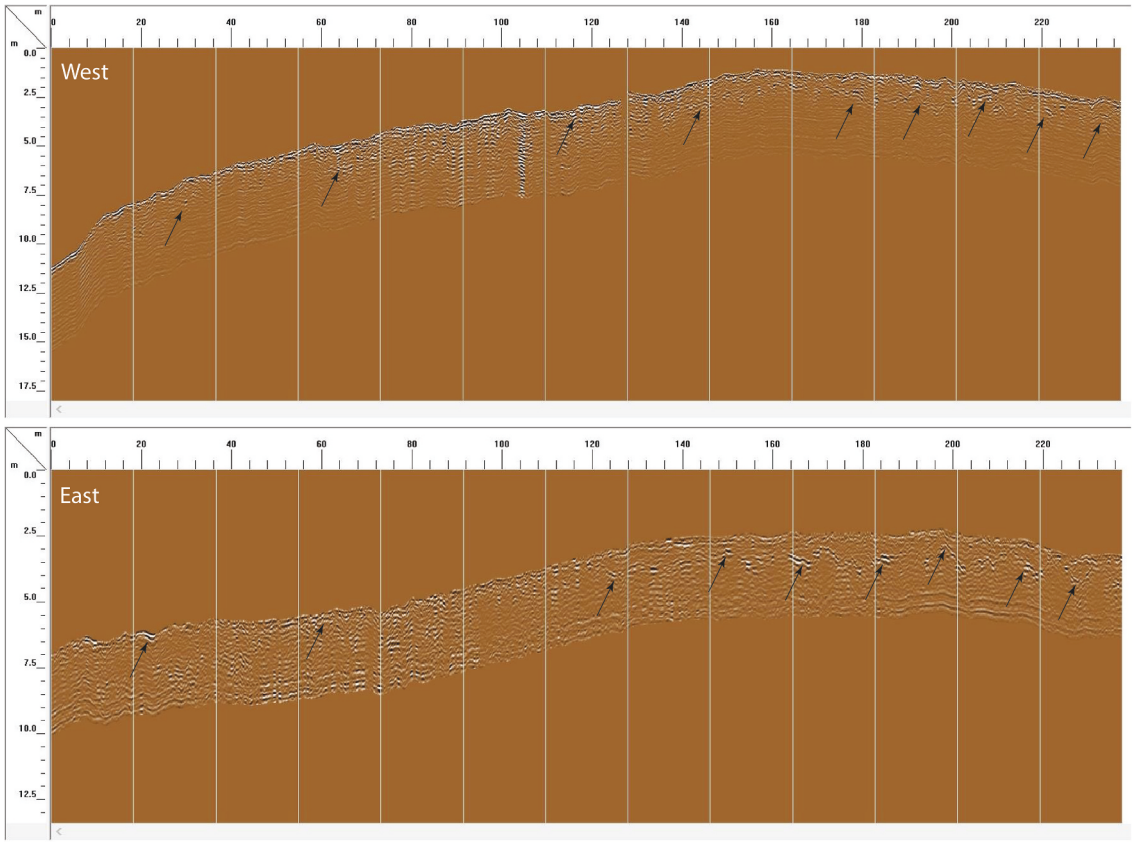

Figure 4. GPR data for the West (top) and East (bottom) transects. Horizontal and vertical scales are in m, and vertical exaggeration is 4.25:1. Arrows highlight the prominent reflector interpreted to be the bedrock surface beneath the regolith. Vertical white lines mark the points measured along the transect at 18-m intervals used to define the horizontal scale.

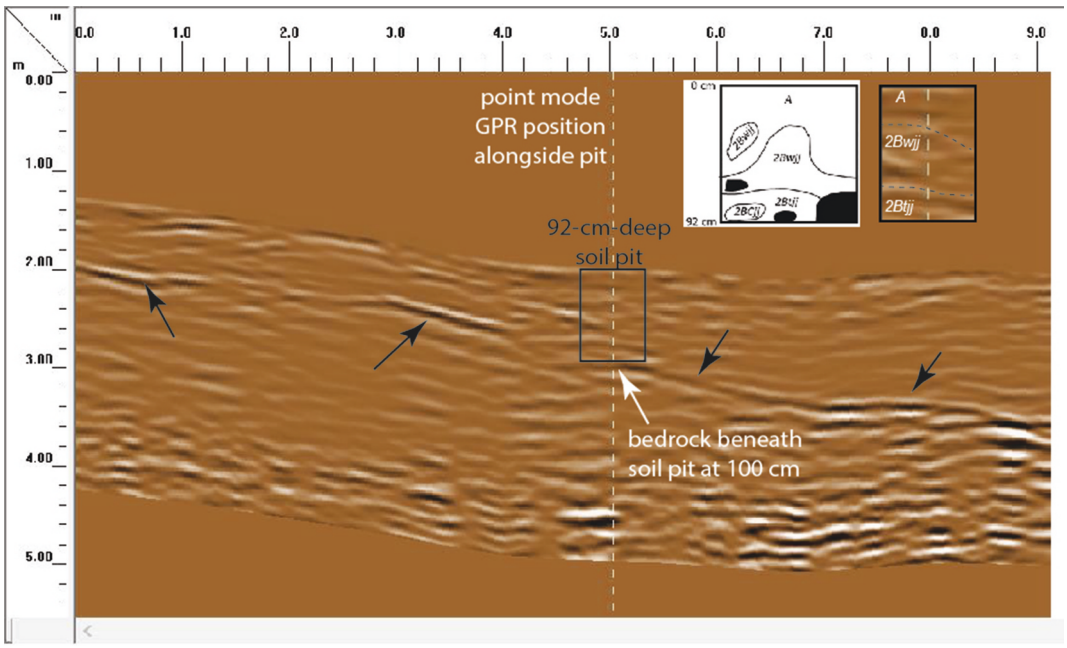

Figure 5. GPR profile for one of the short crossing transects at the soil pit (Figure 3). Arrows highlight the prominent reflector interpreted to be the bedrock surface beneath the regolith. The dashed vertical line marks the center of the soil pit where bedrock was not encountered within 92 cm of the surface; GPR data suggest the bedrock contact is at a depth of ~100 cm. The dimensions of the pit are presented as the black box. Vertical exaggeration is 0.9:1. Upper right shows a field sketch of the cryoturbated soil horizons observed in the pit and a possible correlation to the GPR data.

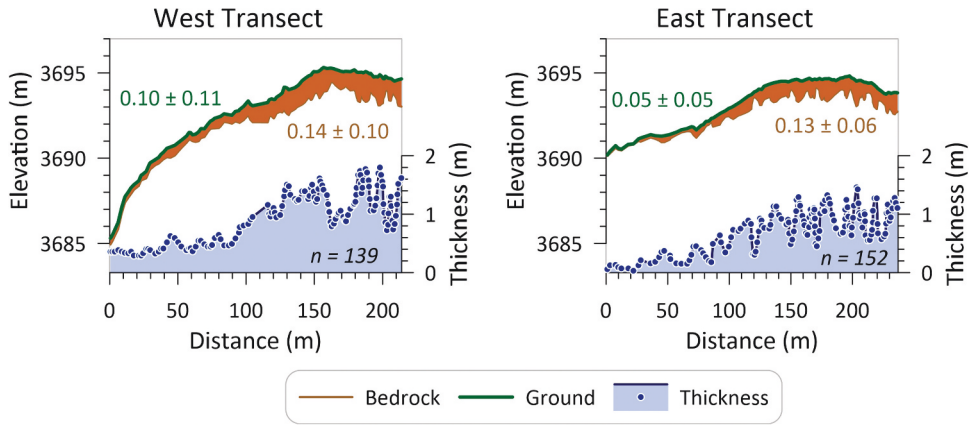

Figure 6. Profiles of the ground surface (green) and regolith (brown) along the West and East transects. Regolith thickness is plotted at the bottom for comparison. Roughness values for the ground surface (green) and bedrock surface (brown) are presented as mean ± 1 standard deviation. Dots on the regolith thickness plot mark points digitized in the GPR data to trace the bedrock-regolith contact (n = number of points along each transect). Vertical exaggeration is 13:1.

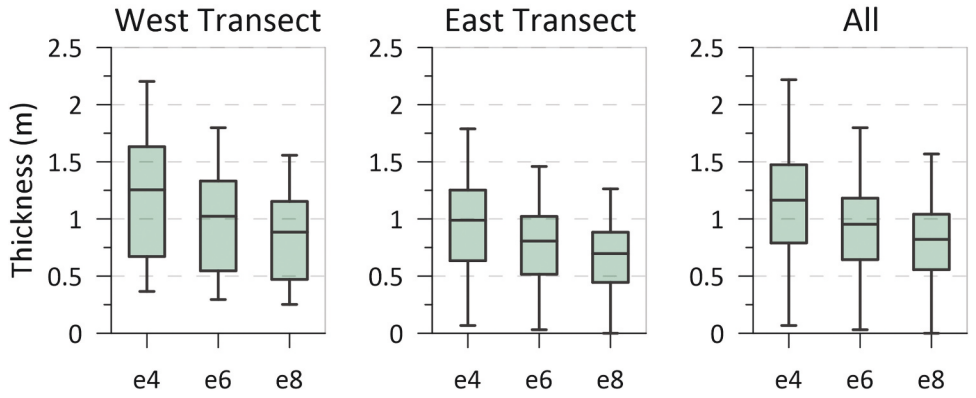

Figure 7. Box and whisker plots of regolith thickness along the West (n = 139) and East (n = 152) transects, as well as for the composite of all measurements at the Chepeta site (n = 369). Thickness was estimated with 3 different values of dielectric permittivity (ε_r): 4, 6 and 8.

than the standard deviation on the depth averages and because repeat digitizing of the reflector position did not produce notably different results.

The reflector interpreted as the bedrock surface exhibits notable irregularity, particularly beneath the higher elevations at the southern end of the transects (Figures 4 and 6). There, depth of the bedrock below the ground surface varies by as much as 30 cm between adjacent measurements along the West transect and 44 cm along the East transect. To evaluate this contrast further, a topographic roughness (R_t) index was calculated as,

$$R_t = [abs(Z_{p-1} - Z_p) + abs(Z_{p+1} - Z_p)] \div 2$$

where Z_p is the elevation of a point, Z_{p-1} is the elevation of the preceding point along the transect, Z_{p+1} is the elevation of the following point along the transect, and *abs* indicates absolute value. Values of R_t average 0.14 ± 0.1 for the bedrock surface compared to 0.07 ± 0.1 for the ground surface, a difference that is statistically significant (t = 8.9, p < .001). Thus, the visibly smooth surface of the soil masks a significantly rougher bedrock surface.

Moreover, roughness of the bedrock surface is not random. A nonparametric runs test (Wald-Wolfowitz test) demonstrates that the presence of fourteen runs relative to the mean in the west transect and twenty runs in the east transect is significant (p < .01), where a run is a string of adjacent regolith thickness estimates consistently above or below the mean value. Particularly beneath the higher elevations, oscillations of the bedrock reflector define irregular waves with an amplitude ≥1 m over lengths of ~10 m (Figure 4). Because the spacing of the points digitized to define the reflector was variable, it is not possible to determine the exact form of the bedrock surface. However, it is clear that this roughness is organized into topography at the multimeter scale that is completely masked by the regolith.

Discussion

Regolith thickness and form of the regolith–bedrock interface

The results of this investigation, comprising half a kilometer of GPS-referenced GPR survey lines, support previous predictions, based on limited data, that regolith thickness on an alpine summit flat is on the order of 1 m. Although estimated thickness varies in response to the selected value of ε_r, using an intermediate value of 6, regolith thickness at the Chepeta site averages ~90 cm (Figure 7). This conclusion supports numerical modeling efforts demonstrating that summit flat regolith thickness stabilizes at ~1 m regardless of original thickness (R. S. Anderson 2002).

Convergence of the thickness at ~1 m reflects that a certain amount of regolith holding water against the bedrock surface accelerates rock weathering, yet too great a thickness of regolith retards weathering by insulating the bedrock from thermal and biogenic disturbances propagating downward from the surface (Gilbert 1877; Heimsath et al. 1999). A thickness of ~1 m, therefore, seems to provide the optimum conditions for bedrock conversion to regolith, at a rate that is balanced by the efficacy of frost creep in moving regolith downslope toward the summit flat edge (R. S. Anderson 2002).

The realization that the thickness of regolith beneath a summit flat surface can vary considerably is a notable outcome of this investigation. Previous work on summit flats, utilizing scattered natural exposures and isolated hand-dug pits, was unable to recognize this smaller scale variability. At the Chepeta site, the standard deviation of thickness measurements (38 cm) is nearly half as large as the mean regolith thickness (91 cm), conveying the degree of variability. Also striking is the full thickness range; although the average thickness is ~90 cm, the minimum is <10 cm and the maximum is nearly 2 m. Thus, whereas the claim that summit flat regolith is thin is confirmed by the GPR data presented here, the parallel assertion that summit flat regolith is uniform in thickness is not supported.

Many models of soil mantled landscapes predict that soil thickness is a function of slope, because downslope diffusion of soil on steeper slopes can happen at rates that are faster relative to soil production (Heimsath et al. 1997). However, although soil thickness at the Chepeta site is generally greater under the crest of the saddle where slopes are gentler (Figure 3), there is no statistically significant relationship between soil thickness and surface slope across the full array of measurements made from the GPR data. Instead, regolith thickness is unrelated to overall slope of the summit flat surface.

Because the ground surface of the Chepeta site is notably smooth (Figure 6), the variability in regolith thickness is a consequence of roughness on the bedrock surface. As seen in Figure 4 and plotted in Figure 6, the bedrock surface, particularly beneath the crest of the summit flat where average regolith thickness is greater, is organized into an irregular pattern of waves with an amplitude ≥1 m over horizontal scales of tens of meters. Because both the West and East transects crossed similar bedrock highs and lows, the pattern on the bedrock surface must be aligned at least somewhat orthogonal to the maximum ground surface slope; if the bedrock ridges paralleled the surface slope, then the GPR transects would not have crossed them. Without a greater density of transects to enable a pseudo three-dimensional investigation of the bedrock surface (Grasmueck, Weger, and Horstmeyer 2005), the true nature of this pattern cannot be discerned. Nonetheless, it is clear that the bedrock surface is not as smooth as the overlying ground.

Previous studies applying geophysics to the mountain CZ provide a context in which to consider the results from the Chepeta site. Leopold et al. (2008) employed GPR and shallow seismic refraction to understand the arrangement of sedimentary units over bedrock above treeline at a site in Colorado. This effort was expanded by later efforts utilizing electrical resistivity tomography at lower elevations nearby (Leopold et al. 2013). Collectively this work, which was conducted across a broader array of topographic settings than the summit flat considered at Chepeta, demonstrates that regolith thickness in non-summit flat locations can be considerably greater; regolith imaged on side slopes at one site in Colorado has a maximum thickness >10 m (Leopold et al. 2008). Moreover, just as at the Chepeta site, regolith thickness in the Colorado studies exhibits considerable lateral variability (Leopold et al. 2008, 2013), and there is no strong correlation between regolith thickness and local surface slope. Similar results have been reported for alpine and non-alpine settings in other studies (Völkel, Leopold, and Roberts 2001; Sauer and Felix-Henningsen 2004; Dethier and Lazarus 2006; Migoń and Kacprzak 2014).

A key distinction between the Colorado studies and the Chepeta site is the report of saprolite atop the bedrock in Colorado. The presence of saprolite was not inferred from the GPR results at the Chepeta site, and none was encountered in the soil pit. Without deeper excavations or boreholes, it is unclear whether deeply weathered material exists here at the regolith–bedrock boundary. On the other hand, the clay-enriched materials locally exposed at the top of the headwall at the northern boundary of the Chepeta site may reflect the existence of saprolite mixed with weathered ash and

mineral dust (Munroe, Ryan, and Proctor 2021). Overall, the spatial variability of regolith thickness inferred at the Chepeta site connects with previous work emphasizing that the mountain CZ can contain a complicated array of spatially variable sedimentary layers over bedrock.

Origin of the regolith

The regolith at the Chepeta site is likely a composite of materials produced by different processes over time. Physical weathering is certain to be an important mechanism for decomposing bedrock and rock fragments at this location. Data from the Chepeta weather station demonstrate a subzero mean annual temperature (−2.8°C in 2019, when only 5 percent of hourly measurements were missing) and frequent oscillations (215 times in 2019) above and below 0°C, which would promote effective freeze–thaw weathering. Rock buried under a certain amount of regolith might also spend more time in the temperature range at which frost cracks expand most rapidly (S. P. Anderson 1988, 2002). Furthermore, water trapped within regolith will migrate toward segregation ice lenses during freeze-up, increasing frost wedging potential (Walder and Hallet 1985). Together these conditions would accelerate frost shattering beyond rates typical for bare bedrock outcrops. Some of the regolith imaged by GPR, therefore, is likely produced through mechanical breakdown of the local bedrock.

A second source for the fine component of the regolith at the Chepeta site is eolian deposition of mineral dust. Dust is currently accumulating at this site at a rate of ~3.3 g/m^2/yr (Munroe 2022). Studies of lacustrine sediment records from elsewhere in the Rocky Mountains indicate that dust fluxes increased as a result of European settlement of the Southwestern United States in the nineteenth century, so it is unclear how representative this modern rate is of fluxes over long timescales. On the other hand, numerous lines of evidence suggest that dust transport and deposition were enhanced under glacial conditions (Petit et al. 1990; Kohfeld and Harrison 2001; Derbyshire 2003; Újvári et al. 2010), so the anthropogenically elevated modern rate might be on the order of the flux that characterized much of the Quaternary when global ice volumes were greater than they are today. Bulk density values of B and C horizons in Uinta alpine soils average 1.5 g/cm^3 (Munroe 2007), and deeper regolith is likely slightly denser (Mouazen, Ramon, and Baerdemaeker 2002). Assuming the dust as deposited has a bulk density half that of the soil (0.75 g/cm^3), a flux of 3.3 g/m^2/yr corresponds to an annual vertical addition of 4.4×10^{-4} cm to each square centimeter of the ground surface. Over a million years, dust would accumulate to 4.4 m. This calculation is rudimentary; however, it emphasizes that dust deposition over Quaternary timescales could contribute substantially to the fine fraction of the regolith present atop the bedrock at the Chepeta site. It is also supported by mixing model analysis estimating that as much 80 percent of the soil (<2 mm size fraction) at the Chepeta site is of eolian origin (Munroe et al. 2020). This insight is notable because dust deposition is known to be an active process in many of the mountain ranges where summit flats are present (e.g., Dahms and Rawlins 1996; Muhs and Benedict 2006), yet dust accumulation was not explicitly considered in prior numerical modeling of summit flat evolution (R. S. Anderson 2002).

Chemical weathering also likely plays a role in the formation of this regolith. Due to the fundamental thermal dependence of weathering reactions, it is typically assumed that chemical weathering is less pronounced under colder conditions (Lasaga 1984; Brady and Carroll 1994). However, dedicated studies have cast doubt on that assertion, revealing that chemical weathering can play a key role in the decomposition of bedrock in Arctic and alpine settings (Dixon, Thorn, and Darmody 2004; Dixon and Thorn 2005). Throughout the alpine zone of the Uintas in general, and at the Chepeta site in particular, field and laboratory investigations have consistently demonstrated an abundance of clay minerals in the alpine soils (Olson 1962; Bockheim and Koerner 1997). Some of these are illite, demonstrated to be a constituent of modern dust (Munroe 2014; Munroe et al. 2015), so not all clays are evidence of local chemical weathering. On the other hand, some soils at the Chepeta site are notably enriched in interstratified kaolinite–illite–smectite, which is not present in the modern dust (Munroe, Ryan, and Proctor 2021). These minerals likely formed in situ through weathering of muscovite and potassium feldspar delivered by eolian activity. Other soils at the Chepeta site contain beidellite, a smectite mineral often produced through weathering of biotite (Munroe, Ryan, and Proctor 2021). The Mg content of these clays (~1.6 percent Mg) is higher than that of modern dust (1.2 percent), despite the tendency of Mg^{2+} to be leached in from soils. Therefore, it has been proposed that these minerals originated through the weathering of biotite-bearing volcanic ash deposited across the Uinta region ~30 Ma during the Oligocene (Kowallis et al. 2005). Collectively, these results support a role for in situ chemical weathering of mineral dust and ash as a third source of regolith at the Chepeta site.

These various contributors to the regolith do not result in a simple stratified deposit with physically weathered rock on the bottom, weathering ash in the middle, and dust closest to the surface. Cryoturbation driven by

the periglacial climate at the Chepeta site is effective at homogenizing these materials over time. Support for this proposition comes from field observations of soils throughout the Uintas, where a uniform layer of loess is present atop landforms of vastly different age (Bockheim et al. 2000). Even in the alpine zone near the Chepeta site, soils in the centers of large sorted polygons, which were presumably active under more rigorous periglacial conditions during Last Glacial Maximum, are mantled by a continuous loess cap (Munroe 2007). This situation suggests that loess accumulates at the soil surface during intervals of landscape stability, such as the modern interglacial, and is mixed into the solum during times of active cryoturbation. Given the general dimensions of the sorted features at the Chepeta site and the relation between patterned ground size and depth of mixing (Hallet and Prestrud 1986), it is reasonable to assume that cryoturbation during glacial times is sufficient to mix the full thickness of this regolith, even if the ground surface is generally stable under interglacial conditions.

Implications for the alpine CZ

Irregularities in bedrock surface beneath alpine summit flats, and the resulting variable regolith thickness, have implications for how the CZ functions in these settings. The weathering processes that form regolith from bedrock (Graham, Rossi, and Hubbert 2010), the mosaic of plant communities on the surface (Meyer et al. 2007), periglacial processes such as cryoturbation (Hallet and Prestrud 1986), and the storage of shallow groundwater (Bales et al. 2011) will all likely be influenced, to at least some degree, by the depth to bedrock. Similarly, variations in regolith thickness mean that thicker regolith may be concentrated in local pockets. These deeper pockets will may slow the lateral movement of soil water (Hahm et al. 2019), possibly slowing chemical weathering by leaching (Wilford and Thomas 2013). Alternatively, in soils prone to moisture deficits, pockets of thicker regolith may retain a larger soil water reservoir, which could benefit plants (Hahm et al. 2019) and possibly enhance weathering reactions (Langston et al. 2011). The influence of many of these effects could be heightened in alpine settings like the Chepeta site with low mean annual temperatures, short growing seasons, and siliciclastic bedrock deficient in nutrients needed by plants. Thus, the irregular bedrock topography at the Chepeta site likely means that the CZ at this location operates differently than it would if the bedrock were as smooth as the overlying ground surface.

Recognition that the bedrock surface beneath an alpine summit flat can be locally irregular also has implications for the history of these landforms. Numerical modeling suggests that summit flats arise through an equilibrium between regolith production and frost creep (R. S. Anderson 2002), regardless of starting condition. Yet at the same time, CZ research across a diverse array of settings has consistently emphasized the important role of landscape history as a control on CZ functioning, as summarized by Guo and Lin (2016). The roughness of the bedrock surface at the Chepeta site, and particularly the apparent concentration of this roughness beneath the ridge crest, is a clue to the longer-term history of this landform. Perhaps the bedrock highs and lows imaged by the GPR represent isolated tors formed during an earlier periglacial interval that were buried by colluvium transported into the saddle from higher topography to the east and west (Figure 1) or were progressively submerged by accumulating ash and dust. Or maybe these local high points are the expression of minor faulting along the crest of the Uinta anticline during Laramide uplift. Alternatively, perhaps weathering reactions beneath the regolith, enhanced by positive feedback processes, have slowly developed topography in situ on a formerly smooth bedrock surface. Evaluating these contrasting interpretations is beyond the scope of this study.

Ultimately, the realization that the thickness of regolith in the alpine CZ is spatially variable, regardless of origin or age, is an important consideration for efforts to understand how the CZ works. As argued by previous work (Leopold et al. 2013), conceptual and numerical modeling of CZ functioning is improved by incorporation of realistic spatial variability of surficial materials (Chaplot et al. 2004; Guo and Lin 2016). Efforts to generate gridded estimates of regolith thickness at large spatial scales are a significant step in this direction (Wald, Graham, and Schoeneberger 2013; Pelletier et al. 2016), yet ground-truthed studies are still needed at the local scale, particularly for settings like the mountain CZ with steep environmental gradients and complicated geologic histories (e.g., Leopold et al. 2013).

Limitations and directions for future work

Although the GPR approach employed here generated orders of magnitude more information about regolith thickness than would be possible by hand excavations, this method does have limitations that should be acknowledged and used to guide future work. The first is that only one summit flat was investigated, and with two primary transects. To expand on the results reported here, similar surveys should be conducted across other summit flats, perhaps with a range of slopes or aspects. The extensive summit flat landscape within the Uintas would provide the opportunity to do this in

locations with generally consistent bedrock lithologies. Expanding this approach to other mountain ranges where summit flats are present would permit the role of lithology and weathering resistance to be investigated.

A second limitation is the reality that a GPR system simply records the two-way travel time of radar waves and that to convert these results into depths requires an estimate of the radar velocity within the regolith. This project took a conservative approach, using a range of velocities (noted by varying ε_r values) plausible for the sandy materials exposed in hand excavations at the Chepeta site. These values were further refined by comparing the GPR results from adjacent to the deep soil pit, where no bedrock was encountered. Therefore, it is likely that these regolith thickness estimates are realistic. Nonetheless, additional investigations to calculate a radar velocity over reflectors of known depth, along with direct calculation of velocity through the common midpoint technique (Jacob and Urban 2016), which was not possible with the bistatic antenna used here, could improve these depth estimates further.

An additional consideration is that GPR is not the only geophysical technique useful for evaluating the stratigraphy of sediments and rock in the shallow CZ. Shallow seismic refraction surveys could be employed in concert with GPR to improve interpretative power (Leopold et al. 2008). Passive seismic techniques are also promising (Stanko and Markušić 2020). This approach was attempted at the Chepeta site, but high wind speeds produced resonance of the seismometer at a frequency similar to that of the underlying soil, making it impossible to calculate regolith thickness. Nonetheless, this approach might be fruitful under more benign weather conditions and should be explored further. Finally, methods for measuring electric resistivity have been shown to be helpful in imaging the CZ and are particularly appropriate for delineating frozen and nonfrozen materials (Leopold et al. 2013). Future work on summit flats in the Uintas and elsewhere would benefit from a combination of these methods.

Conclusion

Ground-penetrating radar surveying reveals that the thickness of regolith overlying the bedrock on an alpine summit flat in the Uinta Mountains (Utah, USA) averages 91 ± 38 cm when calculated with a dielectric permittivity (ε_r) of 6. This result corroborates previous studies proposing that regolith thickness on these landforms is on the order of ~1 m. Regolith thickness exhibits considerable previously unrecognized spatial variability; this realization was made possible by the density and lateral extent of the GPR-derived depth measurements, which greatly exceed what would be possible through even the most laborious physical excavations. Recognition that regolith thickness can vary considerably beneath an alpine summit flat has implications for soil formation, carbon storage, and the transmission and storage of shallow groundwater, as well as evolutionary models for periglacial mountain landscapes.

Acknowledgments

The author thanks S. Munroe for field assistance. Fieldwork took place in the ancestral homelands of the Ute tribe. The article was improved by thoughtful comments from Bob Anderson, Jacob Yde, and an anonymous reviewer.

Disclosure statement

No potential conflict of interest was reported by the author.

Funding

This work was supported by the U.S. National Science Foundation under Grant EAR-201282.

ORCID

Jeffrey S. Munroe http://orcid.org/0000-0002-9356-1899

Data availability

The GPR data collected in this project are available in the open Zenodo repository at https://zenodo.org/badge/DOI/10.5281/zenodo.8302139.svg.

References

Amundson, R., D. D. Richter, G. S. Humphreys, E. G. Jobbágy, and J. Gaillardet. 2007. Coupling between biota and earth materials in the critical zone. *Elements* 3, no. 5: 327–32. doi:10.2113/gselements.3.5.327.

Anderson, R. S. 2002. Modeling the tor-dotted crests, bedrock edges, and parabolic profiles of high alpine surfaces of the Wind River Range, Wyoming. *Geomorphology* 46, no. 1–2: 35–58. doi:10.1016/S0169-555X(02)00053-3.

Anderson, S. P. 1988. Upfreezing in sorted circles, Western Spitsbergen, in 5th International Conference on Permafrost, Trondheim, Norway, p. 666–71.

Anderson, R. S., C. A. Riihimaki, E. B. Safran, and K. R. MacGregor. 2006. Facing reality: Late Cenozoic evolution of smooth peaks, glacially ornamented valleys, and deep river gorges of Colorado's Front Range. In *Tectonics, Climate, and Landscape Evolution*, ed. S. D. Willett, N. Hovius, M. T. Brandon, and D. M. Fisher. Vol. 398, 397–418. Boulder: Geological Society of America. doi:10.1130/2006.2398(25).

Bales, R. C., J. W. Hopmans, A. T. O'Geen, M. Meadows, P. C. Hartsough, P. Kirchner, C. T. Hunsaker, and

D. Beaudette. 2011. Soil moisture response to snowmelt and rainfall in a Sierra Nevada mixed-conifer forest. *Vadose Zone Journal* 10: 786–99. doi:10.2136/vzj2011.0001.

Bockheim, J. G., and D. Koerner. 1997. Pedogenesis in alpine ecosystems of the eastern Uinta Mountains, Utah, USA. *Arctic and Alpine Research* 29, no. 2: 164–72. doi:10.2307/1552043.

Bockheim, J. G., and J. S. Munroe. 2014. Organic carbon pools and genesis of alpine soils with permafrost: A review. *Arctic, Antarctic, and Alpine Research* 46, no. 4: 987–1006. doi:10.1657/1938-4246-46.4.987.

Bockheim, J. G., J. Munroe, D. Douglass, and D. Koerner. 2000. Soil development along an elevational gradient in the southeastern Uinta Mountains, Utah, USA. *Catena* 39, no. 3: 169–85. doi:10.1016/S0341-8162(99)00091-0.

Bradley, W. C. 1987. Erosion surfaces of the Colorado Front Range: A review. *Geomorphic Systems of North America* 2: 215–20.

Bradley, W. H. 1936. *Geomorphology of the north flank of the Uinta Mountains*. Washington, DC: US Government Printing Office.

Brady, P. V., and S. A. Carroll. 1994. Direct effects of CO_2 and temperature on silicate weathering: Possible implications for climate control. *Geochimica et Cosmochimica Acta* 58, no. 7: 1853–6. doi:10.1016/0016-7037(94)90543-6.

Brantley, S. L. 2010. Rock to regolith. *Nature Geoscience* 3, no. 5: 305–6. doi:10.1038/ngeo858.

Brantley, S. L., M. B. Goldhaber, and K. V. Ragnarsdottir. 2007. Crossing disciplines and scales to understand the critical zone. *Elements* 3, no. 5: 307–14. doi:10.2113/gselements.3.5.307.

Brencher, G., A. L. Handwerger, and J. S. Munroe. 2021. InSAR-based characterization of rock glacier movement in the Uinta Mountains, Utah, USA. *The Cryosphere* 15, no. 10: 4823–44. doi:10.5194/tc-15-4823-2021.

Catani, F., S. Segoni, and G. Falorni. 2010. An empirical geomorphology-based approach to the spatial prediction of soil thickness at catchment scale. *Water Resources Research* 46, no. 5. doi:10.1029/2008WR007450.

Chaplot, V., C. Walter, P. Curmi, P. Lagacherie, and D. King. 2004. Using the topography of the saprolite upper boundary to improve the spatial prediction of the soil hydromorphic index. *Geoderma* 123, no. 3–4: 343–54. doi:10.1016/j.geoderma.2004.03.001.

Checketts, H. N., G. T. Carling, D. P. Fernandez, S. T. Nelson, K. A. Rey, D. G. Tingey, C. A. Hale, B. N. Packer, C. P. Cordner, D. B. Dastrup, and Z. T. Aanderud. 2020. Trace element export from the critical zone triggered by snowmelt runoff in a Montane Watershed, Provo River, Utah, USA. *Frontiers in Water* 2: 578677. doi:10.3389/frwa.2020.578677.

Chorover, J., R. Kretzschmar, F. Garcia-Pichel, and D. L. Sparks. 2007. Soil biogeochemical processes within the critical zone. *Elements* 3, no. 5: 321–6. doi:10.2113/gselements.3.5.321.

Czudek, T. 1995. Cryoplanation terraces—a brief review and some remarks. *Geografiska Annaler: Series A, Physical Geography* 77: 95–105. doi:10.1080/04353676.1995.11880431.

Dahms, D. E., and C. L. Rawlins. 1996. A two-year record of eolian sedimentation in the Wind River Range, Wyoming, USA. *Arctic and Alpine Research* 28, no. 2: 210–6. doi:10.2307/1551762.

Davis, J. L., and A. P. Annan. 1989. Ground-penetrating radar for high-resolution mapping of soil and rock stratigraphy. *Geophysical Prospecting* 37, no. 5: 531–51. doi:10.1111/j.1365-2478.1989.tb02221.x.

Dehler, C. M., S. M. Porter, L. D. De Grey, D. A. Sprinkel, and A. Brehm. 2007. The Neoproterozoic Uinta Mountain group revisited; a synthesis of recent work on the Red Pine Shale and related undivided clastic strata, northeastern Utah, U. S. A. In *Special Publication - Society for Sedimentary Geology*, ed. P. K. Link and R. S. Lewis. Vol. 86, 151–66. Tulsa: SPEM Society for Sedimentary Geology.

Derbyshire, E. 2003. Loess, and the Dust Indicators and Records of Terrestrial and Marine Palaeoenvironments (DIRTMAP) database. *Quaternary Science Reviews* 22, no. 18–19: 1813–19. doi:10.1016/S0277-3791(03)00209-9.

Dethier, D. P., and E. D. Lazarus. 2006. Geomorphic inferences from regolith thickness, chemical denudation and CRN erosion rates near the glacial limit, Boulder Creek catchment and vicinity, Colorado. *Geomorphology* 75, no. 3–4: 384–99. doi:10.1016/j.geomorph.2005.07.029.

Dixon, J. C., and C. E. Thorn. 2005. Chemical weathering and landscape development in mid-latitude alpine environments. *Geomorphology* 67, no. 1–2: 127–45. doi:10.1016/j.geomorph.2004.07.009.

Dixon, J. C., C. E. Thorn, and R. G. Darmody. 2004. Measuring the extent of chemical weathering in subarctic alpine environments: Implications for future research. *Polar Geography* 28, no. 1: 63–75. doi:10.1080/789610160.

Doolittle, J. A., B. Jenkinson, D. Hopkins, M. Ulmer, and W. Tuttle. 2006. Hydropedological investigations with ground-penetrating radar (GPR): Estimating water-table depths and local ground-water flow pattern in areas of coarse-textured soils. *Geoderma* 131, no. 3–4: 317–29. doi:10.1016/j.geoderma.2005.03.027.

Doolittle, J. A., D. Surabian, S. McVey, and D. Parizek. 2009. Three "G's" for soil-bedrock depth interpretations. *Soil Survey Horizons* 50, no. 1: 25–30. doi:10.2136/sh2009.1.0025.

Ferrell, R. M., S. Devine, and A. T. O'Geen. 2023. Trends in regolith thickness in a headwater catchment, Sierra Nevada, California. *Vadose Zone Journal* 22, no. 4: e20259. doi:10.1002/vzj2.20259.

Gilbert, G. K. 1877. Report on the geology of the Henry Mountains: U.S. Government Printing Office, 262.

Goodfellow, B. W. 2012. A granulometry and secondary mineral fingerprint of chemical weathering in periglacial landscapes and its application to blockfield origins. *Quaternary Science Reviews* 57: 121–35. doi:10.1016/j.quascirev.2012.09.023.

Graham, R., A. Rossi, and R. Hubbert. 2010. Rock to regolith conversion: Producing hospitable substrates for terrestrial ecosystems. *GSA Today* 20: 4–9. doi:10.1130/gsat57a.1.

Grasmueck, M., R. Weger, and H. Horstmeyer. 2005. Full-resolution 3D GPR imaging. *Geophysics* 70, no. 1: K12–K19. doi:10.1190/1.1852780.

Guo, L., and H. Lin. 2016. Critical zone research and observatories: Current status and future perspectives. *Vadose Zone Journal* 15, no. 9: vzj2016.06.0050. doi:10.2136/vzj2016.06.0050.

Hahm, W. J., D. M. Rempe, D. N. Dralle, T. E. Dawson, S. M. Lovill, A. B. Bryk, D. L. Bish, J. Schieber, and W. E. Dietrich. 2019. Lithologically controlled subsurface critical zone thickness and water storage capacity determine regional plant community composition. *Water Resources Research* 55, no. 4: 3028–55. doi:10.1029/2018WR023760.

Hallet, B., and S. Prestrud. 1986. Dynamics of periglacial sorted circles in Western Spitsbergen. *Quaternary Research* 26, no. 1: 81–99. doi:10.1016/0033-5894(86)90085-2.

Hansen, W. R. 1986. Neogene tectonics and geomorphology of the eastern Uinta Mountains in Utah, Colorado, and Wyoming. *United States Geological Survey, Professional Paper* 75.

Heimsath, A. M., W. E. Dietrich, K. Nishiizumi, and R. C. Finkel. 1997. The soil production function and landscape equilibrium. *Nature* 388, no. 6640: 358–61. doi:10.1038/41056.

Heimsath, A. M., W. E. Dietrich, K. Nishiizumi, and R. C. Finkel. 1999. Cosmogenic nuclides, topography, and the spatial variation of soil depth. *Geomorphology* 27, no. 1–2: 151–72. doi:10.1016/S0169-555X(98)00095-6.

Heimsath, A. M., D. J. Furbish, and W. E. Dietrich. 2005. The illusion of diffusion: Field evidence for depth-dependent sediment transport. *Geology* 33, no. 12: 949–52. doi:10.1130/G21868.1.

Holbrook, W. S., C. S. Riebe, M. Elwaseif, J. L. Hayes, K. Basler-Reeder, D. L. Harry, A. Malazian, et al. 2014. Geophysical constraints on deep weathering and water storage potential in the Southern Sierra Critical Zone Observatory. *Earth Surface Processes and Landforms* 39, no. 3: 366–80. doi:10.1002/esp.3502.

Jacob, R. W., and T. M. Urban. 2016. Ground-penetrating radar velocity determination and precision estimates using common-midpoint (CMP) collection with hand-picking, semblance analysis and cross-correlation analysis: A case study and tutorial for archaeologists. *Archaeometry* 58, no. 6: 987–1002. doi:10.1111/arcm.12214.

Kohfeld, K. E., and S. P. Harrison. 2001. DIRTMAP: The geological record of dust. *Earth-Science Reviews* 54, no. 1–3: 81–114. doi:10.1016/S0012-8252(01)00042-3.

Kowallis, B. J., E. H. Christiansen, E. Balls, M. T. Heizler, and D. A. Sprinkel. 2005. The Bishop Conglomerate ash beds, south flank of the Uinta Mountains, Utah: Are they pyroclastic fall beds from the Oligocene ignimbrites of western Utah and eastern Nevada? *Uinta Mountain Geology, Utah Geological Association* 33: 131–45.

Langston, A. L., G. E. Tucker, R. S. Anderson, and S. P. Anderson. 2011. Exploring links between vadose zone hydrology and chemical weathering in the Boulder Creek critical zone observatory. *Applied Geochemistry* 26: S70–S71. doi:10.1016/j.apgeochem.2011.03.033.

Lasaga, A. C. 1984. Chemical kinetics of water-rock interactions. *Journal of Geophysical Research: Solid Earth* 89, no. B6: 4009–25. doi:10.1029/JB089iB06p04009.

Leopold, M., D. Dethier, J. Völkel, T. Raab, T. C. Rikert, and N. Caine. 2008. Using geophysical methods to study the shallow subsurface of a sensitive alpine environment, Niwot Ridge, Colorado Front Range, U.S.A. *Arctic, Antarctic, and Alpine Research* 40, no. 3: 519–30. doi:10.1657/1523-0430(06-124)[LEOPOLD]2.0.CO;2.

Leopold, M., J. Völkel, J. Huber, and D. Dethier. 2013. Subsurface architecture of the Boulder Creek critical zone observatory from electrical resistivity tomography. *Earth Surface Processes and Landforms* 38, no. 12: 1417–31. doi:10.1002/esp.3420.

Litaor, M. I. 1987. The influence of eolian dust on the genesis of alpine soils in the Front Range, Colorado. *Soil Science Society of America Journal* 51, no. 1: 142–7. doi:10.2136/sssaj1987.03615995005100010031x.

Martinez, A., and A. P. Brynes. 2001. *Modeling dielectric-constant values of geologic materials: An aid to ground-penetrating radar data collection and interpretation*. Lawrence: Kansas Geological Survey.

Mellor, A., and M. J. Wilson. 1989. Origin and significance of gibbsitic montane soils in Scotland, UK. *Arctic and Alpine Research* 21, no. 4: 417–24. doi:10.2307/1551650.

Meyer, M. D., M. P. North, A. N. Gray, and H. S. J. Zald. 2007. Influence of soil thickness on stand characteristics in a Sierra Nevada mixed-conifer forest. *Plant & Soil* 294, no. 1–2: 113–23. doi:10.1007/s11104-007-9235-3.

Migoń, P., and A. Kacprzak. 2014. Lateral diversity of regolith and soils under a mountain slope — Implications for interpretation of hillslope materials and processes, central sudetes. *SW Poland: Geomorphology* 221: 69–82. doi:10.1016/j.geomorph.2014.06.003.

Mouazen, A. M., H. Ramon, and J. D. Baerdemaeker. 2002. SW—soil and water: Effects of bulk density and moisture content on selected mechanical properties of sandy loam soil. *Biosystems Engineering* 83, no. 2: 217–24. doi:10.1006/bioe.2002.0103.

Muhs, D. R., and J. B. Benedict. 2006. Eolian additions to Late Quaternary alpine soils, Peaks Wilderness Area, Colorado Front Range. *Arctic, Antarctic, and Alpine Research* 38, no. 1: 120–30. doi:10.1657/1523-0430(2006)038[0120:EATLQA]2.0.CO;2.

Munroe, J. S. 2006. Investigating the spatial distribution of summit flats in the Uinta Mountains of northeastern Utah, USA. *Geomorphology* 75, no. 3–4: 437–49. doi:10.1016/j.geomorph.2005.07.030.

Munroe, J. S. 2007. Properties of alpine soils associated with well-developed sorted polygons in the Uinta Mountains, Utah, USA. *Arctic, Antarctic, and Alpine Research* 39, no. 4: 578–91. doi:10.1657/1523-0430(06-077)[MUNROE]2.0.CO;2.

Munroe, J. S. 2014. Properties of modern dust accumulating in the Uinta Mountains, Utah, USA, and implications for the regional dust system of the Rocky Mountains. *Earth Surface Processes and Landforms* 39, no. 14: 1979–88. doi:10.1002/esp.3608.

Munroe, J. S. 2018. Distribution, evidence for internal ice, and possible hydrologic significance of rock glaciers in the Uinta Mountains, Utah, USA. *Quaternary Research* 90, no. 1: 1–16. doi:10.1017/qua.2018.24.

Munroe, J. S. 2022. Relation between regional drought and mountain dust deposition revealed by a 10-year record from an alpine critical zone. *Science of the Total Environment* 844: 156999. doi:10.1016/j.scitotenv.2022.156999.

Munroe, J. S., E. C. Attwood, S. S. O'Keefe, and P. J. Quackenbush. 2015. Eolian deposition in the alpine zone of the Uinta Mountains, Utah, USA. *Catena* 124: 119–29. doi:10.1016/j.catena.2014.09.008.

Munroe, J. S., and B. J. Laabs. 2017. Combining radiocarbon and cosmogenic ages to constrain the timing of the last glacial-interglacial transition in the Uinta Mountains, Utah, USA. *Geology* 45, no. 2: 171–4. doi:10.1130/G38156.1.

Munroe, J. S., and B. J. C. Laabs. 2009. Glacial Geologic Map of the Uinta Mountains Area, Utah and Wyoming. Utah Geological Survey Miscellaneous Publication 09-4DM, scale Map.

Munroe, J. S., E. D. Norris, P. M. Olson, P. C. Ryan, M. J. Tappa, and B. L. Beard. 2020. Quantifying the contribution of dust to alpine soils in the periglacial zone of the Uinta Mountains, Utah, USA. *Geoderma* 378: 114631. doi:10.1016/j.geoderma.2020.114631.

Munroe, J. S., P. C. Ryan, and A. Proctor. 2021. Pedogenic clay formation from allochthonous parent materials in a periglacial alpine critical zone. *Catena* 203: 105324. doi:10.1016/j.catena.2021.105324.

Nelson, F. E. 1989. Cryoplanation terraces: Periglacial cirque analogs. *Geografiska Annaler: Series A, Physical Geography* 71, no. 1–2: 31–41. doi:10.1080/04353676.1989.11880271.

Nyland, K. E., and F. E. Nelson. 2020. Time-transgressive cryoplanation terrace development through nivation-driven scarp retreat. *Earth Surface Processes and Landforms* 45, no. 3: 526–34. doi:10.1002/esp.4751.

Obu, J., S. Westermann, A. Bartsch, N. Berdnikov, H. H. Christiansen, A. Dashtseren, R. Delaloye, B. Elberling, B. Etzelmüller, and A. Kholodov. 2019. Northern Hemisphere permafrost map based on TTOP modelling for 2000–2016 at 1 km^2 scale. *Earth-Science Reviews* 193: 299–316. doi:10.1016/j.earscirev.2019.04.023.

Olson, O. C. 1962. Some soil-plant-erosion relationships on the Leidy Peak Uinta alpine area. USDA Forest Service.

Patton, N. R., K. A. Lohse, S. E. Godsey, B. T. Crosby, and M. S. Seyfried. 2018. Predicting soil thickness on soil mantled hillslopes. *Nature Communications* 9, no. 1: 3329. doi:10.1038/s41467-018-05743-y.

Pelletier, J. D., P. D. Broxton, P. Hazenberg, X. Zeng, P. A. Troch, G.-Y. Niu, Z. Williams, M. A. Brunke, and D. Gochis. 2016. A gridded global data set of soil, intact regolith, and sedimentary deposit thicknesses for regional and global land surface modeling. *Journal of Advances in Modeling Earth Systems* 8, no. 1: 41–65. doi:10.1002/2015MS000526.

Petit, J. R., L. Mourner, J. Jouzel, Y. S. Korotkevich, V. I. Kotlyakov, and C. Lorius. 1990. Palaeoclimatological and chronological implications of the Vostok core dust record. *Nature* 343, no. 6253: 56–8. doi:10.1038/343056a0.

Phillips, J. D., D. A. Marion, K. Luckow, and K. R. Adams. 2005. Nonequilibrium regolith thickness in the Ouachita Mountains. *The Journal of Geology* 113, no. 3: 325–40. doi:10.1086/428808.

RADAN v7.6. 2024. Geophysical Survey Systems.

Rea, B. R., W. B. Whalley, M. M. Rainey, and J. E. Gordon. 1996. Blockfields, old or new? Evidence and implications from some plateaus in northern Norway. *Geomorphology* 15, no. 2: 109–21. doi:10.1016/0169-555X(95)00118-O.

Rønning, J. S. 2023. Finetuning ground penetrating radar velocity analysis from hyperbola fitting using migration. *Near Surface Geophysics* 21, no. 3: 171–81. doi:10.1002/nsg.12250.

Sauer, D., and P. Felix-Henningsen. 2004. Application of ground-penetrating radar to determine the thickness of Pleistocene periglacial slope deposits. *Journal of Plant Nutrition and Soil Science* 167, no. 6: 752–60. doi:10.1002/jpln.200421433.

Sears, J., P. Graff, and G. Holden. 1982. Tectonic evolution of lower Proterozoic rocks, Uinta Mountains, Utah and Colorado. *Geological Society of America Bulletin* 93, no. 10: 990–7. doi:10.1130/0016-7606(1982)93<990:TEOLPR>2.0.CO;2.

Small, E. E., and R. S. Anderson. 1998. Pleistocene relief production in Laramide mountain ranges, western United States. *Geology* 26, no. 2: 123–6. doi:10.1130/0091-7613(1998)026<0123:PRPILM>2.3.CO;2.

Small, E. E., R. S. Anderson, and G. S. Hancock. 1999. Estimates of the rate of regolith production using ^{10}Be and ^{26}Al from an alpine hillslope. *Geomorphology* 27, no. 1–2: 131–50. doi:10.1016/S0169-555X(98)00094-4.

Small, E. E., R. S. Anderson, J. L. Repka, and R. Finkel. 1997. Erosion rates of alpine bedrock summit surfaces deduced from in situ ^{10}Be and ^{26}Al. *Earth and Planetary Science Letters* 150, no. 3–4: 413–25. doi:10.1016/S0012-821X(97)00092-7.

Sprenger, M., C. Stumpp, M. Weiler, W. Aeschbach, S. T. Allen, P. Benettin, M. Dubbert, A. Hartmann, M. Hrachowitz, and J. W. Kirchner. 2019. The demographics of water: A review of water ages in the critical zone. *Reviews of Geophysics* 57, no. 3: 800–34. doi:10.1029/2018RG000633.

Stanko, D., and S. Markušić. 2020. An empirical relationship between resonance frequency, bedrock depth and V_{S30} for Croatia based on HVSR forward modelling. *Natural Hazards* 103, no. 3: 3715–43. doi:10.1007/s11069-020-04152-z.

Thorn, C. E., and K. Hall. 2002. Nivation and cryoplanation: The case for scrutiny and integration. *Progress in Physical Geography* 26, no. 4: 533–50. doi:10.1191/0309133302pp351ra.

Újvári, G., J. Kovács, G. Varga, B. Raucsik, and S. B. Marković. 2010. Dust flux estimates for the Last Glacial Period in East Central Europe based on terrestrial records of loess deposits: A review. *Quaternary Science Reviews* 29, no. 23–24: 3157–66. doi:10.1016/j.quascirev.2010.07.005.

Völkel, J., M. Leopold, and M. C. Roberts. 2001. The radar signatures and age of periglacial slope deposits, Central Highlands of Germany. *Permafrost and Periglacial Processes* 12, no. 4: 379–87. doi:10.1002/ppp.402.

Walder, J., and B. Hallet. 1985. A theoretical model of the fracture of rock during freezing. *Geological Society of America Bulletin* 96, no. 3: 336–46. doi:10.1130/0016-7606(1985)96<336:ATMOTF>2.0.CO;2.

Wald, J. A., R. C. Graham, and P. J. Schoeneberger. 2013. Distribution and properties of soft weathered bedrock at ≤ 1 m depth in the contiguous United States. *Earth Surface Processes and Landforms* 38, no. 6: 614–26. doi:10.1002/esp.3343.

Waroszewski, J., K. Kalinski, M. Malkiewicz, R. Mazurek, G. Kozlowski, and C. Kabala. 2013. Pleistocene–Holocene cover-beds on granite regolith as parent material for Podzols — An example from the Sudeten Mountains. *Catena* 104: 161–73. doi:10.1016/j.catena.2012.11.006.

Wilford, J., and M. Thomas. 2013. Predicting regolith thickness in the complex weathering setting of the central Mt. Lofty Ranges, South Australia. *Geoderma* 206: 1–13. doi:10.1016/j.geoderma.2013.04.002.